

Supporting Information: The emphasis of interfacial effects in the impedance of nanostructured solid polymer electrolytes

Martino Airoldi, Ullrich Steiner,* and Ilja Gunkel

*Adolphe Merkle Institute, University of Fribourg, Chemin des Verdiers 4, 1700 Fribourg,
Switzerland*

E-mail: ullrich.steiner@unifr.ch

Table S1: Water contact angles of stainless steel and silicon substrates, a random copolymer P(S-*r*-2VP) brush covered silicon wafer, and PS, PEO homopolymer surfaces.

Substrate	Water contact angle [°]
Stainless steel, uncoated	62
Silicon wafer (SW), uncoated	35
P(S- <i>r</i> -2VP)-coated SW	80
PS	99
PEO	42
As-cast SEO (<i>r</i> = 8% LiTFSI) on a pristine SW	53
As-cast SEO (<i>r</i> = 8% LiTFSI) on a P(S- <i>r</i> -2VP) covered SW	66

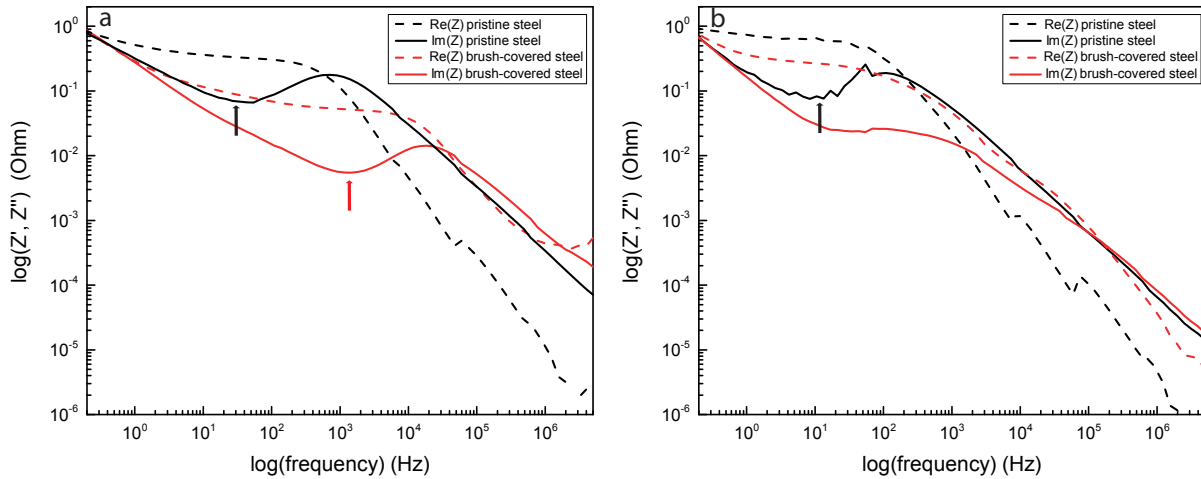


Figure S1: Real and imaginary parts of the complex impedance plotted versus frequency for the SEO BCP cast onto stainless steel (a) and a silicon wafer (b), showing both pristine (black trace) and random copolymer-covered (red trace) surfaces. Electrode polarization on the steel surface is evident in the minima, indicated by the arrows pointing to the imaginary traces. The interfacial polarization is reduced for the brush-covered silicon wafer substrate (continuous red line in b). A similar minimum in the imaginary component is observed for the pristine silicon substrate (continuous black line in b), induced by the preferential wetting of one the BCP phases of the electrode surface. This preferential wetting causes a layered arrangement of the BCP at the surface, localising lithium ions, that are coordinated with the PEO BCP near the surface, mimicking the charge buildup characteristic of the steel substrate.

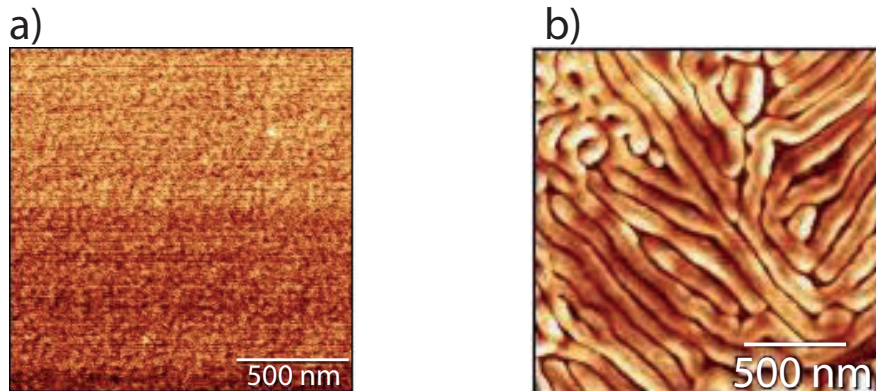


Figure S2: AFM phase images of drop cast SEO9094 with 8% LiTFSI onto an untreated silicon wafer (a) and PS-r-P2VP copolymer brush modified silicon substrate (b).

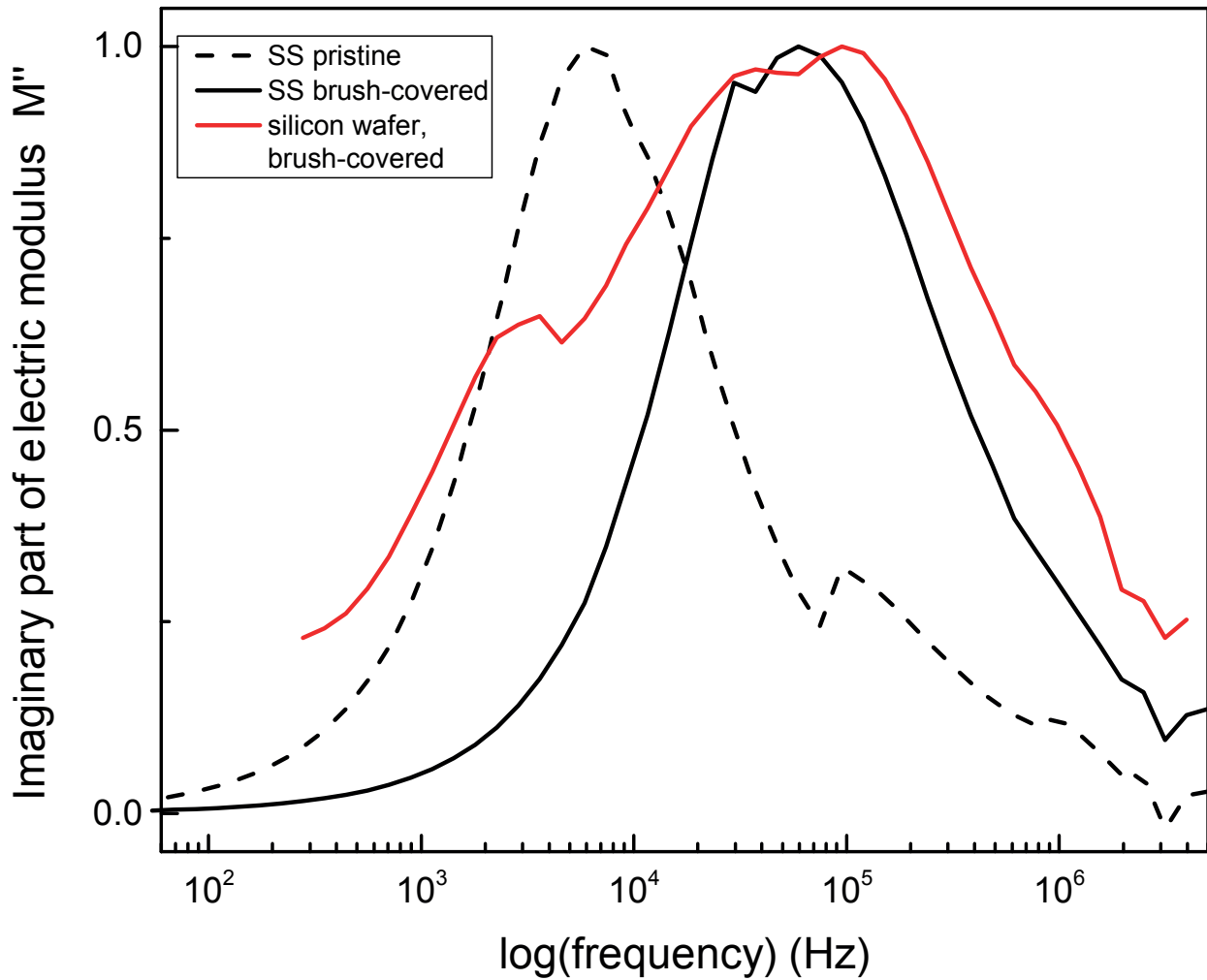


Figure S3: Imaginary component of the electric modulus, M'' , plotted versus frequency of the BCP, measured at 95 °C. Samples sandwiched between pristine and brush-covered stainless steel (dashed and continuous black lines, respectively) are compared to brush-covered silicon electrodes (red).

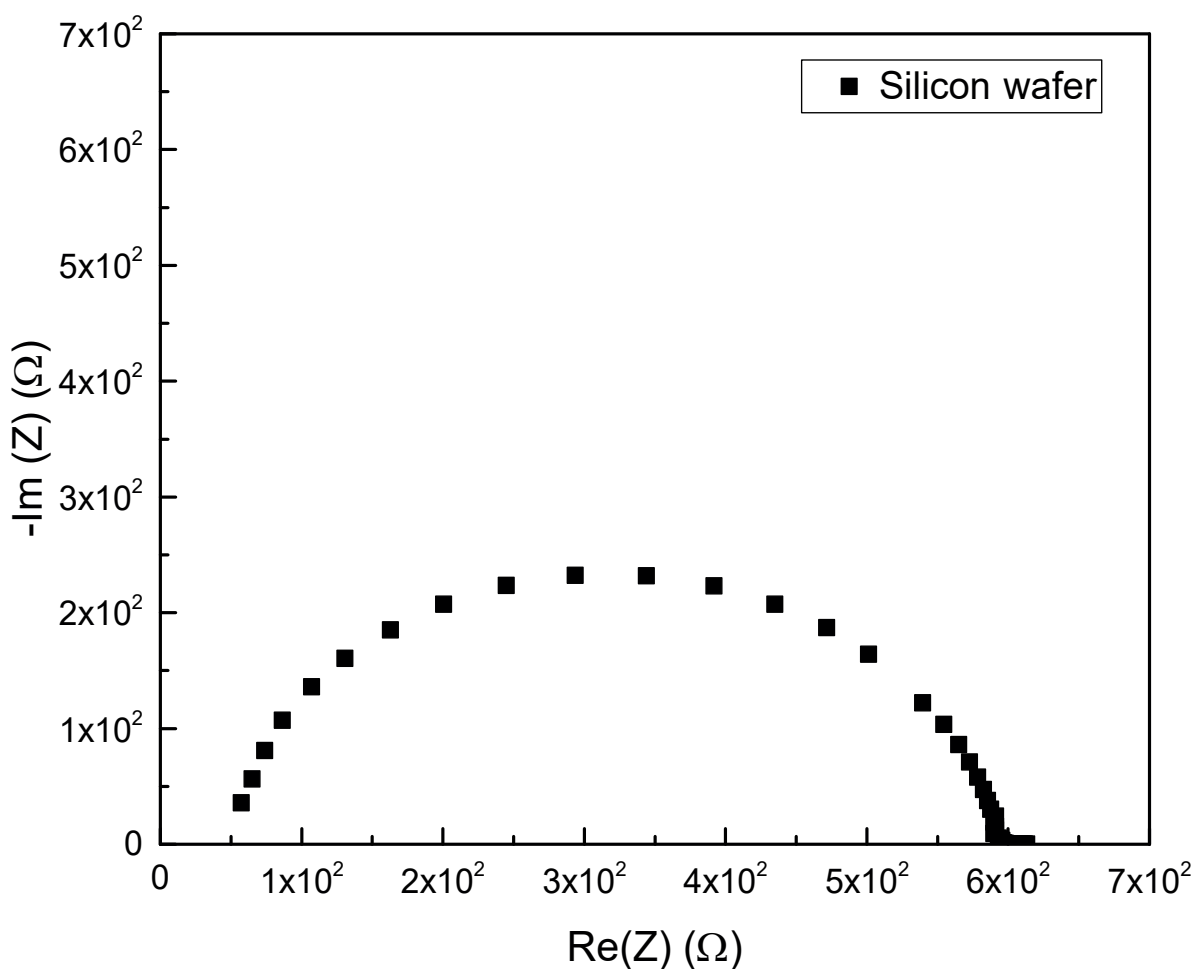


Figure S4: Nyquist plot of a pristine silicon wafer measured between two steel electrodes.

Table S2: Thermal stability of the chemical bonding of the random P(*S*-*r*-2VP) copolymer to the substrate is demonstrated by water contact angle measurements. The brush covered substrates were exposed to three solvents, which were allowed to evaporate at room temperature and in a vacuum oven set to 160 °C , followed by water contact angle measurements at room temperature. While the contact angles were slightly lower after tetrahydrofuran treatment compared to the other two solvents, they were not affected by the high temperature exposure.

Solvent	Water contact angle [°]	
	Ambient temperature	160 °C
Chloroform	89.13	89
Tetrahydrofuran	85.3	84
Anisole	88.68	89.7

Table S3: Nyquist fit parameters (resistance, capacitance, and the a -value associated to the CPE element) of the BCP sandwiched between pristine and brush-covered stainless steel electrodes, compared to PEO 100 kg/mol homopolymer doped with $r = 8\%$ LiTFSI sandwiched between pristine stainless steel electrodes. The value of a varies between zero for a resistor and one for an ordinary capacitor. $a = 0.5$ for a Warburg element. The a -values are close to one for all samples.

Substrate	$R_{\text{SPE}} [\Omega]$	$C_{\text{CPE}} [\text{Fs}^{(a-1)}]$	a
BCP, pristine stainless steel, 22 °C	$82.08e^6 \pm 16.95$	$69.53e^{-12} \pm 32.11e^{-15}$	0.9861
BCP, pristine stainless steel, 35 °C	$9.915e^6 \pm 16.95$	$73.71e^{-12} \pm 0.2555e^{-15}$	0.9532
BCP, pristine stainless steel, 50 °C	$1.896e^6 \pm 1.255$	$45.5e^{-12} \pm 0.7466e^{-15}$	0.9999
BCP, pristine stainless steel, 65 °C	$1.207e^6 \pm 0.6024$	$48.89e^{-12} \pm 0.7022e^{-15}$	0.9984
BCP, pristine stainless steel, 80 °C	$0.887935e^6 \pm 0.2359$	$51.05e^{-12} \pm 1.3194e^{-15}$	0.9933
BCP, pristine stainless steel, 95 °C	$0.705328e^6 \pm 0.7582$	$47.65e^{-12} \pm 1.281e^{-15}$	0.9971
BCP, brush-covered stainless steel, 22 °C	$3.185e^6 \pm 0.8582$	$94.86e^{-12} \pm 0.773e^{-15}$	0.9629
BCP, brush-covered stainless steel, 35 °C	$7.92245e^5 \pm 0.6624$	$81.71e^{-12} \pm 1.845e^{-15}$	0.9773
BCP, brush-covered stainless steel, 50 °C	$1.88374e^5 \pm 0.7267$	$85.02e^{-12} \pm 8.992e^{-15}$	0.9797
BCP, brush-covered stainless steel, 65 °C	$1.11844e^5 \pm 0.8778$	$92.46e^{-12} \pm 20.47e^{-15}$	0.9732
BCP, brush-covered stainless steel, 80 °C	$0.75587e^5 \pm 0.9065$	$91.68e^{-12} \pm 28.13e^{-15}$	0.9764
BCP, brush-covered stainless steel, 95 °C	$0.63641e^5 \pm 0.8983$	$69.43e^{-12} \pm 31.17e^{-15}$	1
PEO, pristine stainless steel, 22 °C	$1.358e^6 \pm 1.096$	$50.49e^{-12} \pm 0.9471e^{-15}$	1
PEO, pristine stainless steel, 35 °C	$0.302075e^6 \pm 0.664$	$53.81e^{-12} \pm 3.828e^{-15}$	0.9972
PEO, pristine stainless steel, 50 °C	$0.041674e^6 \pm 1.086$	$50.38e^{-12} \pm 46.68e^{-15}$	1
PEO, pristine stainless steel, 65 °C	$0.002739e^6 \pm 0.4001$	$51.27e^{-12} \pm 44.65e^{-15}$	1
PEO, pristine stainless steel, 80 °C	$0.001575e^6 \pm 0.363$	$49.5e^{-12} \pm 1.2591e^{-15}$	0.9933
PEO, pristine stainless steel, 95 °C	$0.0009953e^6 \pm 3.313$	$58.12e^{-12} \pm 2.69e^{-12}$	0.9981

Table S4: Nyquist fit parameters of the BCP sandwiched between pristine and brush-covered silicon wafer electrodes.

Substrate	$R_{\text{SPE}}^1 [\Omega]$	$C_{\text{CPE}}^1 [\text{F}_{\text{S}}^{(a-1)}]$	a^1	$R_{\text{SPE}}^2 [\Omega]$	$C_{\text{CPE}}^2 [\text{F}_{\text{S}}^{(a-1)}]$	a^2
pristine silicon, 22 °C	$1.35653e^6 \pm 5.63$	$0.2291e^{-9} \pm 26.56e^{-12}$	0.943	$4.423e^6 \pm 20.19$	$0.3109e^{-9} \pm 28.54e^{-12}$	0.9083
pristine silicon, 35 °C	$0.12649e^6 \pm 4.30$	$14.48e^{-9} \pm 2.253e^{-12}$	0.8923	$1.37713e^6 \pm 66.19$	$0.7367e^{-9} \pm 0.799e^{-12}$	0.8396
pristine silicon, 50 °C	$0.02025e^6 \pm 1.13$	$53.18e^{-9} \pm 47.87e^{-12}$	0.9316	$0.84791e^6 \pm 25.78$	$0.2702e^{-9} \pm 0.3606e^{-12}$	0.9332
pristine silicon, 80 °C	$0.01387e^6 \pm 6.37$	$22.71e^{-9} \pm 15.51e^{-12}$	0.8909	$0.07425e^6 \pm 26.25$	$0.3724e^{-9} \pm 5.73e^{-12}$	0.993
pristine silicon, 95 °C	$0.007928e^6 \pm 5.98$	$0.2148e^{-9} \pm 5.734e^{-12}$	0.9474	$0.07106e^6 \pm 19.52$	$0.3352e^{-9} \pm 21.4e^{-12}$	0.9341
brush-covered silicon, 22 °C	$1.833e^6 \pm 47.04$	$10.32e^{-12} \pm 59.84e^{-15}$	0.9246	$2.397e^6 \pm 170.7$	$4.141e^{-9} \pm 1.911e^{-12}$	0.7675
brush-covered silicon, 35 °C	$0.564675e^6 \pm 51.1$	$78.65e^{-12} \pm 30.95e^{-15}$	0.8356	$0.324383e^6 \pm 45.77$	$2.586e^{-9} \pm 4.266e^{-12}$	0.9108
brush-covered silicon, 50 °C	$0.092174e^6 \pm 81.5$	$69.56e^{-12} \pm 14.8e^{-15}$	0.7832	$0.296144e^6 \pm 60.63$	$1.136e^{-9} \pm 34.4e^{-12}$	0.8764
brush-covered silicon, 65 °C	$0.073811e^6 \pm 170.7$	$18.82e^{-12} \pm 5.154e^{-15}$	0.7777	$0.050889e^6 \pm 47.04$	$0.6574e^{-9} \pm 12.41e^{-12}$	0.9986
brush-covered silicon, 80 °C	$0.046650e^6 \pm 87.74$	$4.141e^{-12} \pm 1.911e^{-15}$	0.7675	$0.25453e^6 \pm 47.04$	$0.1049e^{-9} \pm 59.84e^{-12}$	0.9246
brush-covered silicon, 95 °C	$0.013771e^6 \pm 13.21$	$96.46e^{-12} \pm 11.75e^{-15}$	0.9282	$0.37384e^6 \pm 12.02$	$0.2265e^{-9} \pm 47.95e^{-12}$	0.8899

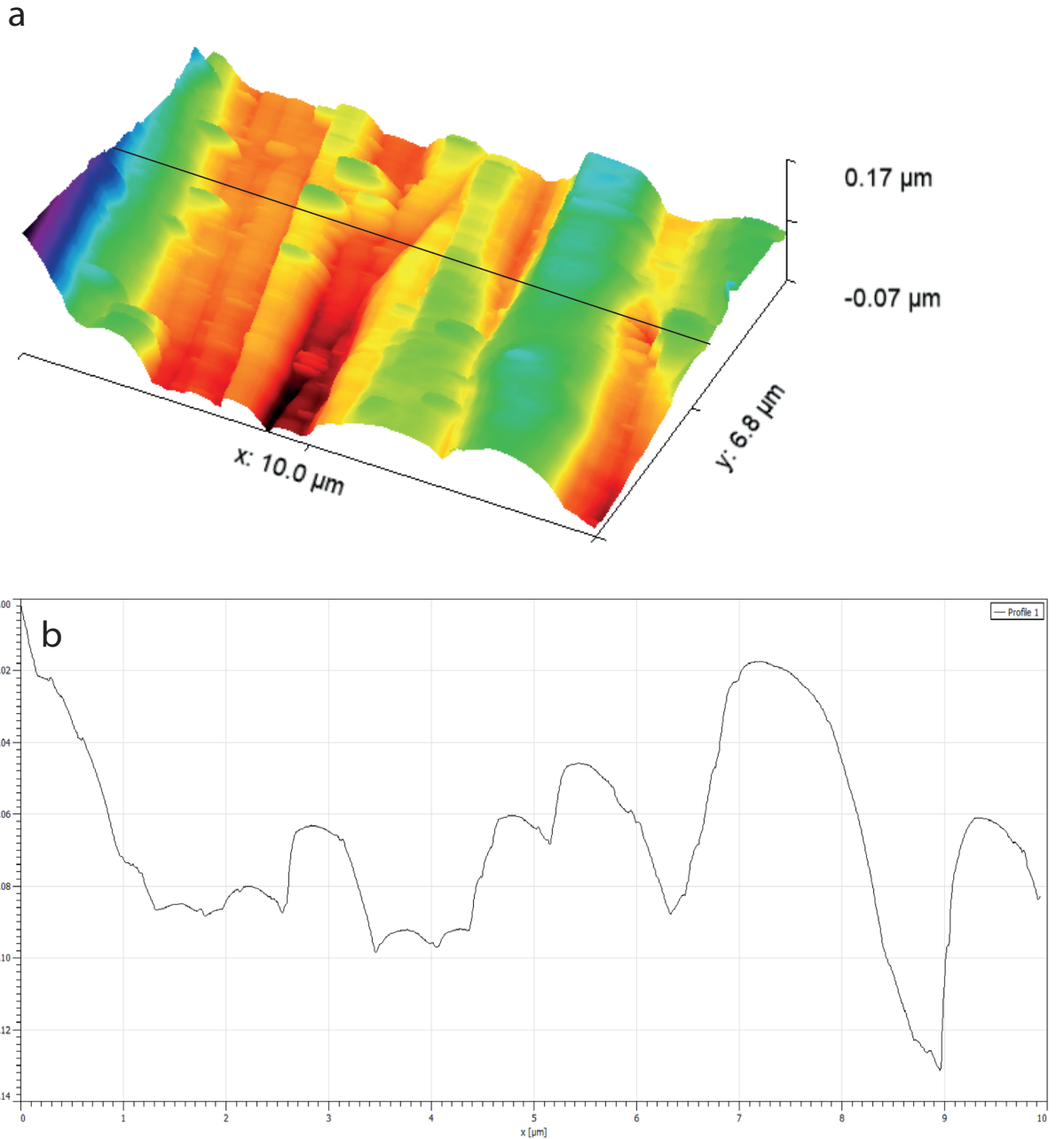


Figure S5: AFM image of the surface of a polished stainless steel disk (**a**), and a profile extraction (**b**), marked by the black line in (a).

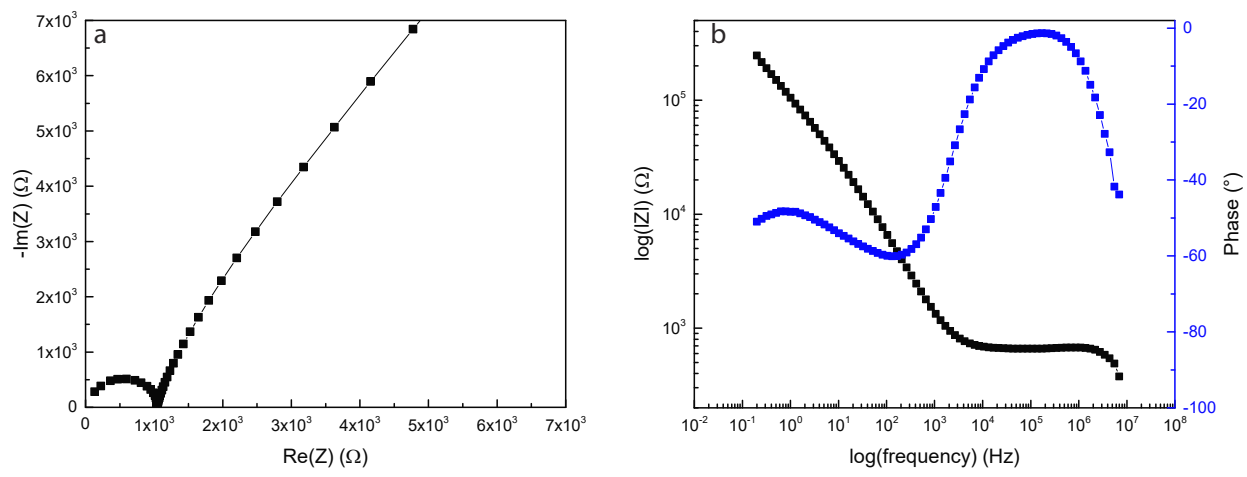


Figure S6: Nyquist plot of the reference PEO homopolymer ($M_w^{\text{PEO}} = 100 \text{ kg/mol}$) (a), and the respective Bode plot (b).

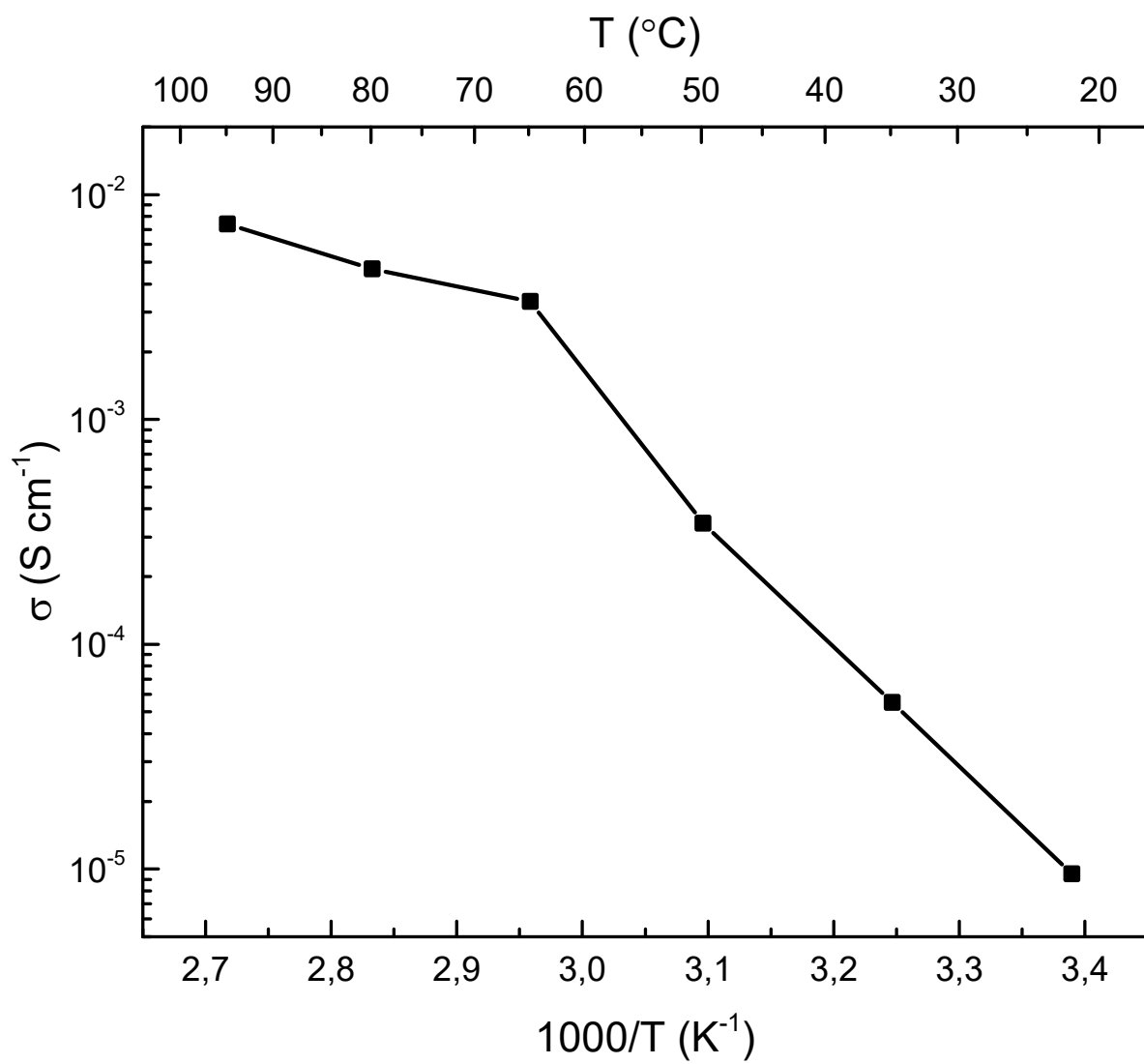


Figure S7: The ionic conductivity vs. temperature plot of the reference PEO homopolymer ($M_w^{\text{PEO}} = 100 \text{ kg/mol}$). A comparison of the conductivities of PEO homopolymer sandwiched between pristine and brush-covered stainless steel substrates is published in ref.¹ (Figure S2).

References

- (1) Sutton, P.; Bennington, P.; Patel, S. N.; Stefk, M.; Wiesner, U. B.; Nealey, P. F.; Steiner, U.; Gunkel, I. Surface Reconstruction Limited Conductivity in Block-Copolymer Li Battery Electrolytes. *Advanced Functional Materials* **2019**, *29*.